XL CILAMCE
IBERO-LATIN AMERICAN CONGRESS ON COMPUTATIONAL METHODS IN ENGINEERING
NOVEMBER 11-14, 2019
Praiamar Natal Hotel & Convention Natal, RN-BRAZIL

NONLINEAR DYNAMIC STUDY OF A SIMPLIFIED SOLAR SAIL STRUCTURE

Lucas Sardinha de Arruda[1]
Reyolando M.L.R.F Brasil[2]
[1]*arrudalucas@usp.br*
[2]*reyolando.brasil@ufabc.edu.br*
[1]*Universidade de São Paulo*
Av. Prof. Almeida Prado, trav.2 nº. 83, Edifício Paula Souza (Prédio da Engenharia Civil), São Paulo, Brasil.
[2]*Universidade Federal do ABC*
Alameda da Universidade, s/nº, Bairro Anchieta, São Bernardo do Campo, Brasil.

Abstract. We propose a nonlinear dynamic study of a solar sail model, to understand the structural response of large lightweight appendages in space environment and to set an adequate procedure to simulate one. Initially, a static linear/nonlinear analysis is carried out using the commercial software ABAQUS® and an implemented nonlinear algorithm to determine the limit conditions of this structure. After that, we perform a dynamic simulation in order to determine the real impact of the nonlinear assumption in the final response of this lightweight model. The numerical algorithm is written in MATLAB® language and based on a 'composite scheme', where the first sub-step solution is obtained via the trapezoidal rule, and for the second sub-step solution, a 3-point Euler backward formula is employed. The dynamic equilibrium at each load step is achieved via a path following methodology, seeking to solve the nonlinear systems of equations derived from the time integration procedure. The proposed 450m^2 solar sail is modelled as a kite-shape structure, consisting of four-swallow lattice members kept in the cross configuration by guyed cables, each one modeled with nonlinear space truss elements. To represent working conditions, solar wind pressure is applied at the upmost elements of the lattice members in conjunction with a set of concentrated forces at the corners of the cross configuration to represent the cables linking the appendage to a supposed mother spacecraft/satellite.

Keywords: Nonlinear Dynamic Analysis; Nonlinear truss; Solar Sail.

1 Introduction

The concept of solar sailing can be traced back to the early 20th century, see Tsander [1], and is based on the phenomenon of the Solar Radiation Pressure (or SRP), were the electromagnetic radiation originated by a solar source perturbs the attitude of spacecraft through conservation of momentum. This perturbation affects every object in sightline, and therefore is perceived regardless of the Spacecraft's orientation. In theory, this concept can outperform conventional systems, such as, chemical and ion propulsion, due to its absence of embarked propellant. The main setback of this concept is that the momentum carried by solar radiation is extremely small, and thus to provide a suitably propulsion an extremely large surface area is needed. A first concept study of solar orientation control was performed by NASA in its Comet Halley mission (Macdonald [2]) and culminated with the Japan Aerospace Exploration Agency spacecraft "IKAROS".

In his work, Tsuda [3] describes the detail behind the Japanese deep space demonstration spacecraft, focusing in explaining the spacecraft design, control systems and solar sail deployment operation, as shown in Figure 1. The mission was launched in May 2010, together with a climate orbiter satellite, as payload of the H-IIA vehicle from the Tanegashima space center. The main objective of this mission was to check the viability of "solar sailing" concept, as well as, test new technologies and procedures, such as, the deployment procedure of the solar sail, demonstration of the guidance and navigation control and power generation using thin film cells embedded in the sail.

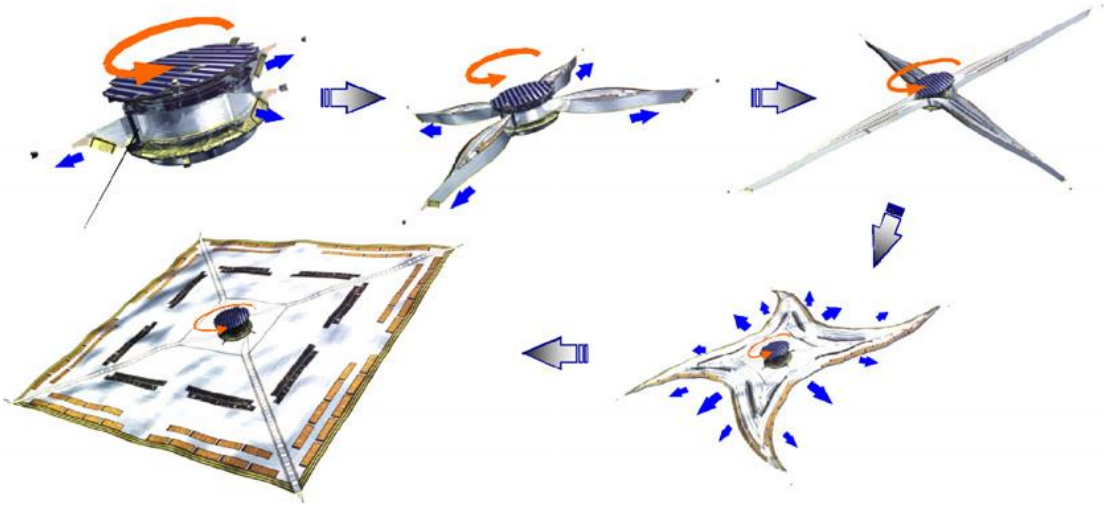

Figure 1. Example of a Solar Sail deployment procedure, Tsuda [3].

In parallel with those concept study missions, a large number of solar sail mission, material technologies and deployment procedures have been devised and promoted by solar sail proponents. In the literature, simulation based on the finite element methods were develop to study the dynamic effects of the typical mission's load envelope, as seeing in Liu [4], in conjunction with alternative formulation and methodologies to improve the current state-of-the-art software's, such as NASTRAN®, ABAQUS® or ANSYS® (Boni [5]). The main objective of this mission was to check the viability of "solar sailing" concept, as well as, test new technologies and procedures, such as, the deployment procedure of the solar sail, demonstration of the guidance and navigation control and power generation using thin film cells embedded in the sail. Finally, this work proposes a nonlinear dynamic study of a solar sail model, to understand the structural response of large lightweight appendages in space environment and to set an adequate procedure to simulate one.

2 Methodology

This section presents a brief introduction about the integration time scheme used to perform the dynamic simulation, as well as, the nonlinear path-following algorithm used to solve the equilibrium equations obtained at each time step. Additionally, we introduce the reader to the nonlinear geometric space truss theory and a short description of the ABAQUS® software.

2.1 "Composite" Time Integration procedure.

The implemented "composite" time integration scheme was proposed by Bathe [6] as an alternative to the classic Newmark method for large displacements and long dynamic responses structural analysis. The main idea behind this scheme is calculate the unknown variables by considering the time step Δt as two equally sized sub-steps. In the first sub-step, the Newmark constant average acceleration method is used to compute the variables value at $t + \Delta t/2$. Then, this solutions in employed in the 3-point Euler backward formula to obtain the new equilibrium state at $t + \Delta t$. In other words, the method uses the solution obtained from the Newmark method as an additional information for the Euler backward formula, correcting and improving its results. For this reason, this simple and efficient procedure is a second-order accurate scheme with small amplitude decay and period elongation and can be directly employed when the mechanical energy is not conserved.

Assuming that for a n-set of nonlinear equilibrium equation with fixed mass matrix $\boldsymbol{m}$ and damping matrix $\boldsymbol{c}$, the dynamic equilibrium equations at the end of a time step $t + \Delta t$ may be expressed as Eq. (1).

$$\boldsymbol{m}\ddot{\boldsymbol{u}}_{tf} + \boldsymbol{c}\dot{\boldsymbol{u}}_{tf} + \boldsymbol{f}_{int} = \boldsymbol{f}_{ext}, \tag{1}$$

where $\boldsymbol{f}_{ext}$ is the equivalent external forces. In the first sub-step, the nodal variables at time $t + \Delta t/2$ are computed via an iterative scheme presented below, see Eq. (2).

$$\begin{gathered}\left(\frac{16}{\Delta t^2}\boldsymbol{m} + \frac{4}{\Delta t}\boldsymbol{c} + \boldsymbol{k}_T^{i-1}\right)_{t+\Delta t/2} \Delta \boldsymbol{u}^{\boldsymbol{i}} = \cdots \\ \left(\boldsymbol{f}_{ext} - \boldsymbol{f}_{int}^{i-1}\right)_{t+\Delta t/2} - \boldsymbol{m}\left(\tfrac{16}{\Delta t^2}\left(u_{t+\Delta t/2}^{i-1} - u_t\right) - \tfrac{8}{\Delta t}\dot{u}_t - \ddot{u}_t\right) - \boldsymbol{c}\left(\tfrac{4}{\Delta t}\left(u_{t+\Delta t/2}^{i-1} - u_t\right) - \dot{u}_t\right),\end{gathered} \tag{2}$$

where $u_{t+\Delta t/2}^{i} = u_{t+\Delta t/2}^{i-1} + \Delta u^{i}$. Thereafter, the second sub-step requires the solution of the previous equilibrium point (t) and the nodal variables at time $t + \Delta t/2$ to obtain the increment displacement at time step $t + \Delta t$ via an iterative scheme using the 3-point backward Euler method, as follows:

$$\begin{gathered}\left(\frac{9}{\Delta t^2}\boldsymbol{m} + \frac{3}{\Delta t}\boldsymbol{c} + \boldsymbol{k}_T^{i-1}\right)_{t+\Delta t} \Delta \boldsymbol{u}^{\boldsymbol{i}} = \left(\boldsymbol{f}_{ext} - \boldsymbol{f}_{int}^{i-1}\right)_{t+\Delta t} + \cdots \\ -\boldsymbol{m}\left(\tfrac{9}{\Delta t^2}u_{t+\Delta t}^{i-1} - \tfrac{12}{\Delta t^2}u_{t+\Delta t/2} + \tfrac{8}{\Delta t^2}u_t - \tfrac{4}{\Delta t}\dot{u}_{t+\Delta t/2} + \tfrac{1}{\Delta t}\dot{u}_t\right) - \boldsymbol{c}\left(\tfrac{3}{\Delta t}u_{t+\Delta t}^{i-1} - \tfrac{4}{\Delta t}u_{t+\Delta t/2} + \tfrac{1}{\Delta t}u_t\right).\end{gathered} \tag{3}$$

2.2 Incremental-iterative numerical procedure

On structural analysis, the Newton-Raphson method is the first-choice technique to solve the set of nonlinear equations obtained at each time step from an applied integration time scheme, mainly due to its simplicity, robustness and second order convergence ratio. Nonetheless, this method and its variants tends to become inefficient when directly applied to problems with a high degree of nonlinearity. A typical solution to overcome this limitation is to treat the load parameter as additional variable, basis of the path-following strategies, such as the Orthogonal residual algorithm or the Arc-length algorithm. (Crisfield [7,8] and Carrera [9])

The main idea behind the Arc-length method is to propose additional constraint equation that aims to find the intersection between the governing equations and an n-dimensional sphere with a fixed radius Δl, thus turning the whole system into a solvable one. In the spherical version of the method, this constraint is given by,

$$\Delta \boldsymbol{u}^T \Delta \boldsymbol{u} + \Delta\lambda^2 \varphi^2 \boldsymbol{f}_{ext}{}^T \boldsymbol{f}_{ext} - \Delta l = 0, \tag{4}$$

being $\Delta \boldsymbol{u}$ is the incremental displacement, $\Delta\lambda$ the incremental load factor and φ the scaling parameter.

A simple explanation of the method can be found in Figure 2, where from a previous equilibrium point (point A), we determine an initial displacement increment δu_t^i based on a tangent estimative (same as the classic Newton-Raphson procedure), leading to the Tangential solution from point A. This initial guess is then corrected by an iterative process based on the constraint equation Eq. (4) until the final solution is achieved.

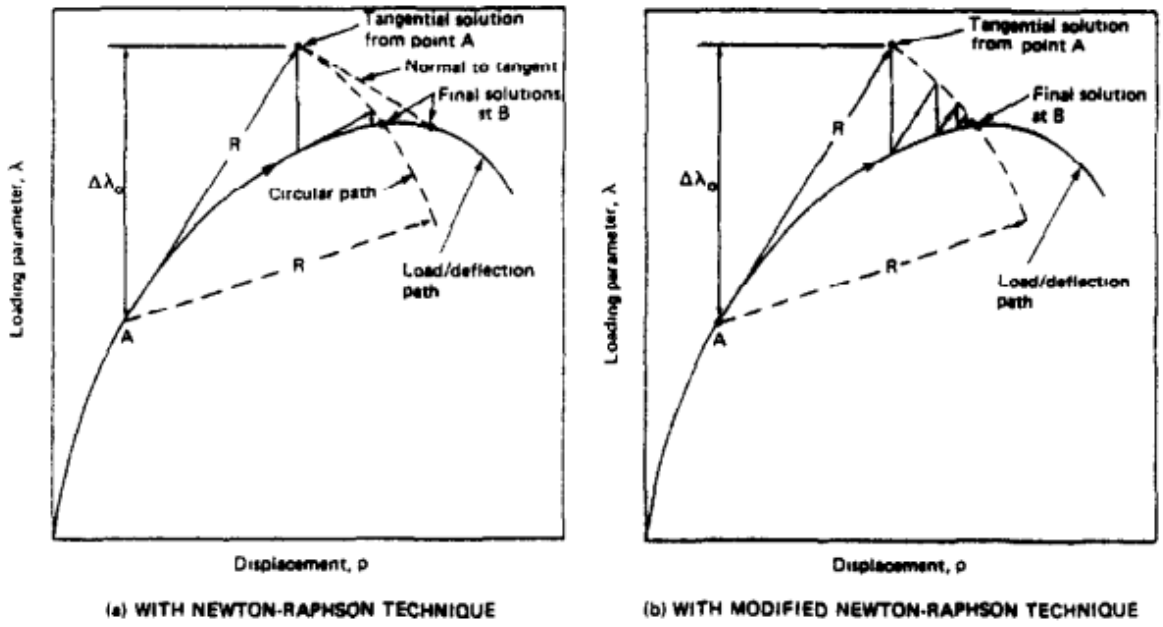

Figure 2. Arc-length methodology based on Newton-Raphson method, Crisfield [7].

Following the formulation proposed by Crisfield, we have that the iterative change of displacement for the new unknown load level is written as:

$$\delta \boldsymbol{u} = -(\boldsymbol{k_t})^{-1}[\boldsymbol{g}^i + \delta\lambda^i \boldsymbol{f}_{ext}] = \overline{\delta \boldsymbol{u}}^i + \delta\lambda^i \delta \boldsymbol{u}_t^i. \tag{5}$$

Being $\boldsymbol{g}^i = \boldsymbol{f}_{int} - \lambda \boldsymbol{f}_{ext}$ is the iterative out of balance array for the static context. Consequently, the incremental displacement $\Delta \boldsymbol{u}_n^{i+1}$ and incremental load $\Delta\lambda^{i+1}$ for the next step can be written as Eq. (6) and Eq. (7).

$$\Delta u_n^{i+1} = \Delta u_n^i + \delta \boldsymbol{u}; \tag{6}$$

$$\Delta\lambda_n^{i+1} = \Delta\lambda_n^i + \delta\lambda^i. \tag{7}$$

Substituting the relations above into the constraint equation, Eq. (4), a quadratic constraint equation arises, given by:

$$a_1(\delta\lambda^i)^2 + a_2\delta\lambda^i + a_3 = 0. \tag{8}$$

The parameters a_1, a_2 and a_3 are constants computed based on the current iterative displacement and load level and are fully presented in Crisfield [7]. The solution of Eq. (8) gives us two possible solution for the new load increment $\delta\lambda^i$, with the possibility of two identical roots; two distinct real roots or complex roots. To avoid the problems of incorrect root choice, Crisfield proposed to choose the appropriate root by estimating the two angles between the displacement vector at the last load increment and the displacement at the current iteration; and choosing the one that gives a positive angle (or closest to the linear solution).

2.3 Nonlinear geometric space truss theory

The fundamental idea behind the nonlinear geometric space truss theory can be traced back to the works of Turner (1960) and Argris (1964), as described in Souza Lima [10], and are widely established in the literature. In this paper, we follow the matrix description presented in Pimenta [11], due to its simplicity and adaptability to nonlinear material models.

Assuming a generic truss bar element in its global reference frame, as shown in Figure 3, we designate V^s, A^s and l^s as its volume, cross section area and length in state s - either the reference state or the current one.

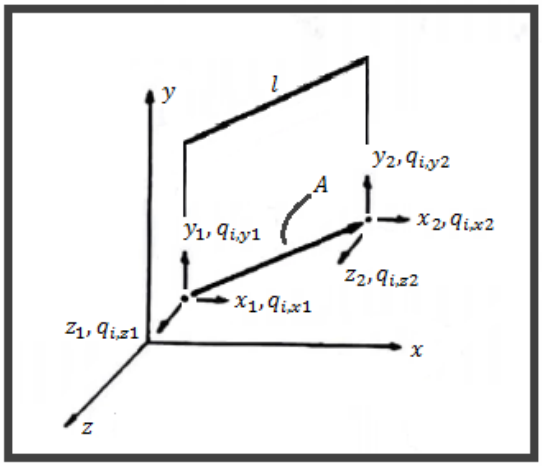

Figure 3. Truss element bar in the global reference frame, Pimenta [11].

In this configuration, the element nodal array is presented as,

$$\boldsymbol{x}_e = \{\{x, y, z\}_1, \{x, y, z\}_2\}^T, \tag{9}$$

where $\{x, y, z, \}_{i=1,2}$ refers to each set of nodal coordinates. Therefore, the element length l^s and its stretch λ^* can be determined using the following relations:

$$l^s = \boldsymbol{x}_e^T \boldsymbol{\phi}^T \boldsymbol{\phi} \boldsymbol{x}_e; \tag{10}$$

and,

$$\lambda^* = (l^{crt}/l^{ref}) = (\sqrt{\boldsymbol{x}_e^T \boldsymbol{\phi}^T \boldsymbol{\phi} \boldsymbol{x}_e})/l^{ref}, \tag{11}$$

where $\boldsymbol{\phi}$ is a matrix relating the two element nodes and given by $\boldsymbol{\phi} = [-\boldsymbol{I}_3 \quad +\boldsymbol{I}_3]$, with $\boldsymbol{I}_3$ representing the 3x3 identity matrix; the superscripts ^{crt} and ^{ref} are related to the current state and the reference one, respectively.

Adopting a linear constitutive relation and a family of strain relations, it is possible to derive the element internal force and stiffness matrix, as

$$\boldsymbol{f}_{int,e} = V^{ref} \sigma^m \lambda^{*2m} (l^{crt})^{-2} \boldsymbol{\phi}^T \boldsymbol{\phi} \boldsymbol{x}_e; \tag{12}$$

and,

$$\begin{aligned} \boldsymbol{K}_{T,e} = \; & V^{ref} \lambda^{*4m} (l^{crt})^{-4} E \boldsymbol{\phi}^T (\boldsymbol{\phi} \boldsymbol{x}_e)(\boldsymbol{\phi} \boldsymbol{x}_e)^T \boldsymbol{\phi} + \cdots \\ & + V^{ref} \lambda^{*2m} [(2m-2) l^{crt\,-4} \sigma^m \boldsymbol{\phi}^T (\boldsymbol{\phi} \boldsymbol{x}_e)(\boldsymbol{\phi} \boldsymbol{x}_e)^T \boldsymbol{\phi} + l^{crt\,-2} \sigma^m \boldsymbol{\phi}^T \boldsymbol{\phi}]. \end{aligned} \tag{13}$$

where E is the elastic modulus of the structure and m a parameter related to the strain-stretch relation. Notice that this procedure can be easily adapted to be a piecewise elastic tangent modulus of a material nonlinear model.

2.4 ABAQUS FEA® software

The ABAQUS FEA® is a software suite for finite element analysis and computer-aided engineering. It has a simple and comprehensive interface that allows the modelling and simulation of complex designs and behaviors. The suite has a broad set of finite element models, optimized explicit and implicit schemes for nonlinear analysis and state-of-the-art procedures to solve contact, thermodynamic and electromagnetic problems. Nonetheless, the software allows for scripting and customization of element and material model subroutines using the computer language Python. Finally, it has a series of packages and interfaces to communicate with third-party programs, e.g. SolidWorks®, Mathematica® or MATLAB®.

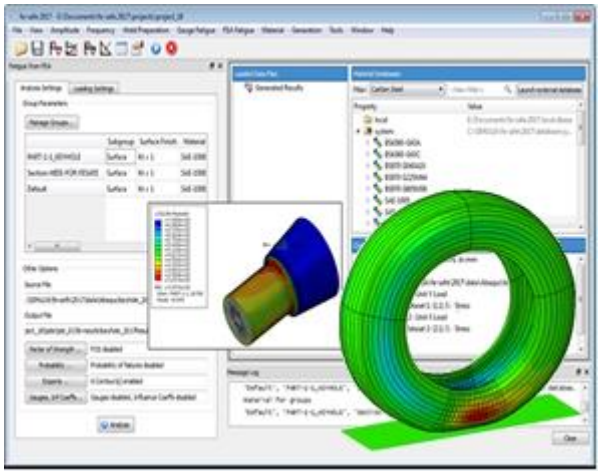

Figure 4. ABAQUS interface example, Company's website [16].

3 Solar Sail Model

In this work, a $450m^2$ kite-shape solar sail is modelled as a four-swallow lattice structure, responsible for the structural shape and stability of the sail, four identical isosceles triangular sails, responsible for the satellite movement and attitude control, and a rigid body element located in the center of the lattice structure and representing the satellite, as shown in Figure 5. In the static analysis performed via ABAQUS®, the complete structure ($Sail + Lattice\ structure$) is adopted, however, for the dynamic counterpart, only the lattice structure is used.

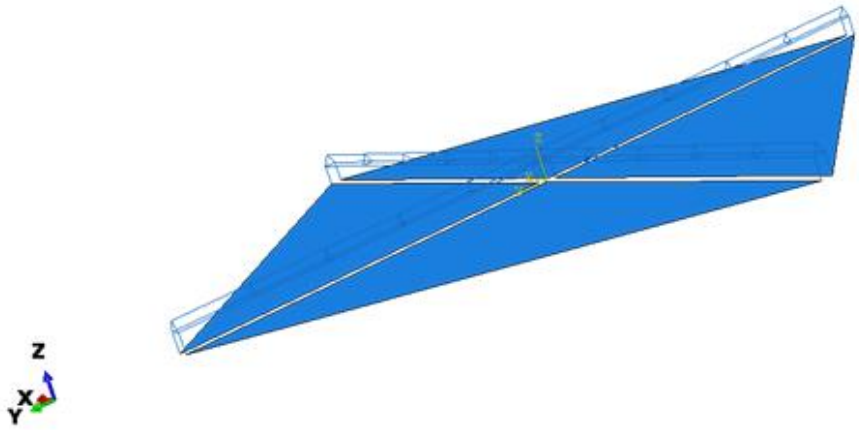

Figure 5. Kite-shape structure model.

The material's mechanical properties used in this study are presented in Table 1. As we can see, from figure 8 and table 1, the transversal truss elements of the lattice structure were based on an E glass fabric class of Carbon Fiber Reinforced Polymer (CFRP) in order to ensure the high-performance and lightweight of the structure. Meanwhile, the triangular shaped rings were modelled using a heavier and sturdier MgAl alloy, in order to prevent buckling of the transversal loaded members and maintains the original lattice shape. The Solar sail was modelled using Polyimide®, same class of high-performance polymers used in the "IKAROS" spacecraft.

Table 1. Material properties.

Material	Density $[kg/m^3]$	Elastic Modulus $[GPa]$	Poisson's ratio
Carbon Fiber Reinforced Polymer	1800	22.0	0.3
MgAl Alloy	1900	45.0	0.29
Polyimide®	1340	2.5	0.37

Table 2 presents the geometric properties of each element type, where should be noticed that the adopted shell element, used to describe the solar sail, is based on the Homogenous shell element model preset in ABAQUS® and uses five integration points for the thickness. Furthermore, a previous set of simulation were performed to set the distance between each ring, as well as, the maximum size of each transversal member.

Table 2. Geometric properties.

Section	Thickness $[m]$	Cross-section area $[m^2]$
Truss	-	2.545E-4
Δ-shaped Ring	-	3.5E-4
Solar sail	1E-05	-

Figure 6 shows the tip section of the four-swallow lattice structure. Each lattice structure has $15\ m$ and consists of fifteen Δ-shaped rings, a 3-element pyramid tip and fifteen Z-section repetitions, each one containing six truss - three in the vertical configuration and three in the diagonal one.

Figure 6. Representation of a single section of the four-swallow lattice structure.

The Solar sail is modelled as four $15m \times 15m$ isosceles triangles, each one representing a quarter of the sail, as see in Figure 7. This representation of the problem allows different set of constraint conditions between the sail and lattice structure, as well as, simplifying the meshing procedure.

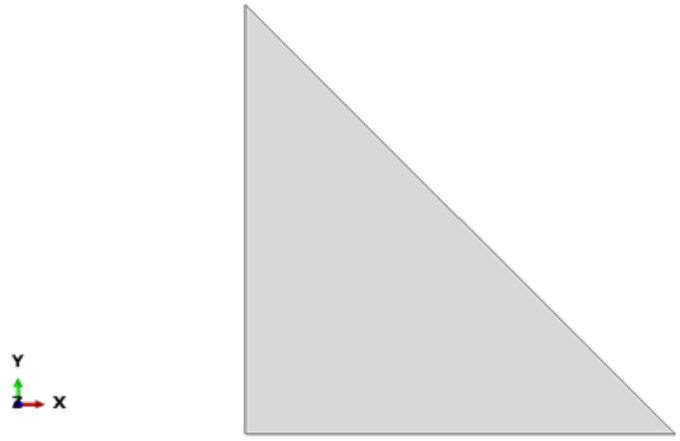

Figure 7. Model of the upper quarter of the solar sail.

For the static analysis, we assume that the cross shaped structure is constraint by the satellite fuselage (assumed rigid) and not allowed for displacement in the three main directions. This is performed by restricting the degrees of freedom of the central part of the lattice, as shown in the left part of Figure 8. Meanwhile, the constraint conditions between the sail and lattice structure are simulated using the axial connection element from ABAQUS®.

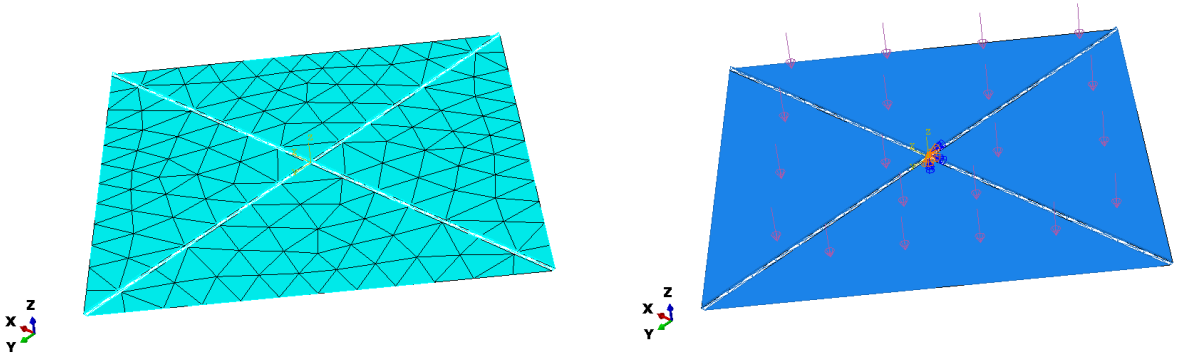

Figure 8. Kite-shape structure model.

The applied pressure at each simulation is presented on Table 3, assuming three possible configurations. The first one being an orbital mission near the Earth; the second one near Venus, similar to the one performed by the "IKAROS" and the third one on the vicinities of Mercury.

Table 3. Solar radiation pressure on perfect reflector at normal incidence, extracted from literature.

Distance from sun	Radiation pressure $[\mu N/m^2]$
0.39 AU (Mercury)	60.6
0.72 AU (Venus)	17.4
1.00 AU (Earth)	9.08

At last, the nonlinear static and dynamic study using the proposed methodology was performed assuming a symmetry condition of the four-swallow lattice structure, being the modelled as a lattice structure presented in Figure 9, this was made to improve the computational efficiency.

Figure 9. Lattice structure model.

4 Results

In this section, we present the static results of the solar sail for three different Solar Radiation Pressure conditions - Earth, Mercury and Venus orbit; and the dynamic nonlinear analysis of exceptional load conditions applied at the tip of the single arm lattice structure presented in Figure 9. This load condition was chosen due to the small displacements observed in the three previous simulations.

4.1 Solar Pressure at 1AU (Earth)

The first simulation consists of a static analysis using the software ABAQUS of the complete model, that is, $Solar\ sail + Lattice$ near the Earth's orbit.

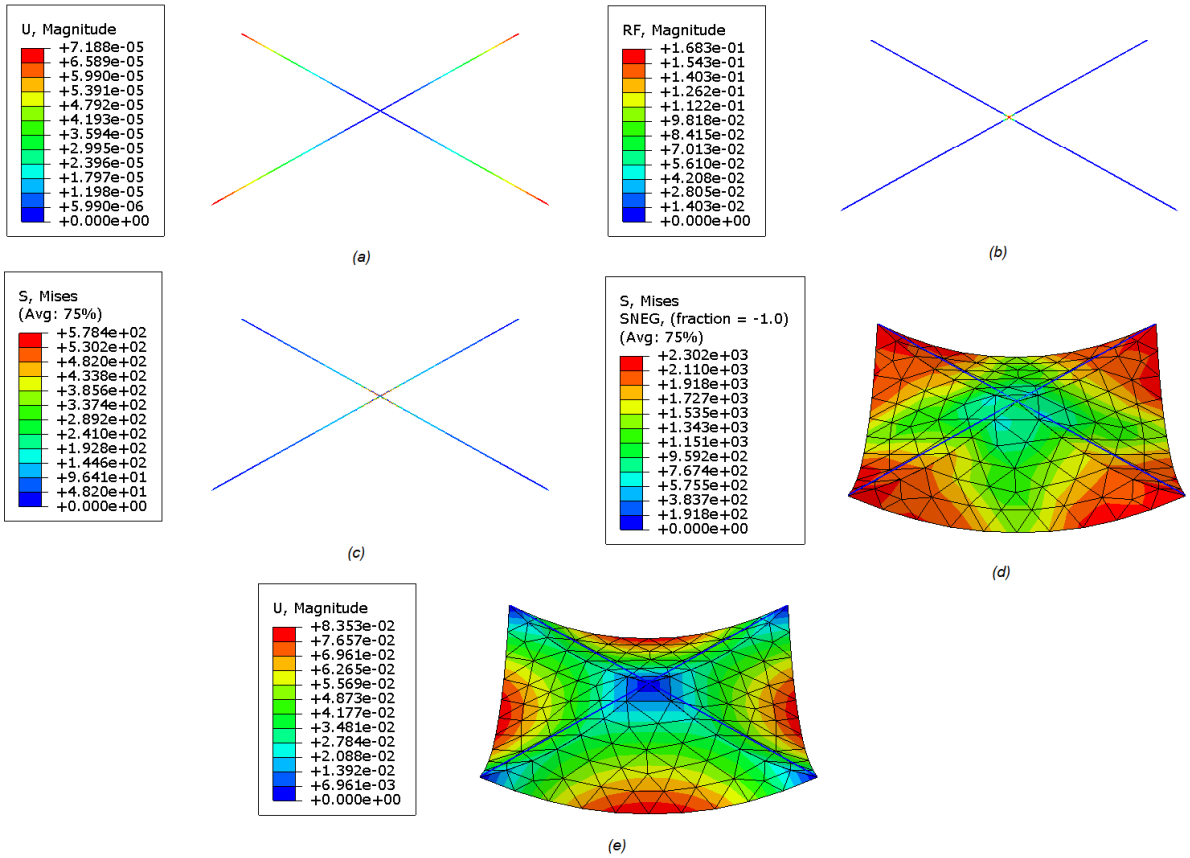

Figure 10. Solar sail analysis near the Earth orbit, where the (a), (b) and (c) illustrations represent the lattice displacement, reaction force and stress respectively; and (d) and (e) the structure stress and displacement.

In this orbit, the maximum pressure value for a perfect reflector at normal incidence is 9.08 $\mu N/m^2$. Applying this pressure at the modelled solar panel results in a maximum displacement magnitude of 71.88 μm at the tip of the lattice structure, as seen in the plots (a) to (e) of Figure 10.

From Fig.10 (d), it is possible to notice that instability effects, specially buckling, should be considered due to the slenderness ration of the truss elements and the compressible stress magnitude noticed in the structural elements near the center, close to the satellite fuselage. Those effects were added to the simulation in a previous study were the position of the MgAl alloy rings were defined, seeking to optimize the load-distance ratio.

4.2 Solar Pressure at 0.72AU (Venus)

For the second simulation, a distance of 0.7 astronomical units is adopted, representing a satellite mission near the Venus's orbit, similar to the one performed by the spacecraft "IKAROS".

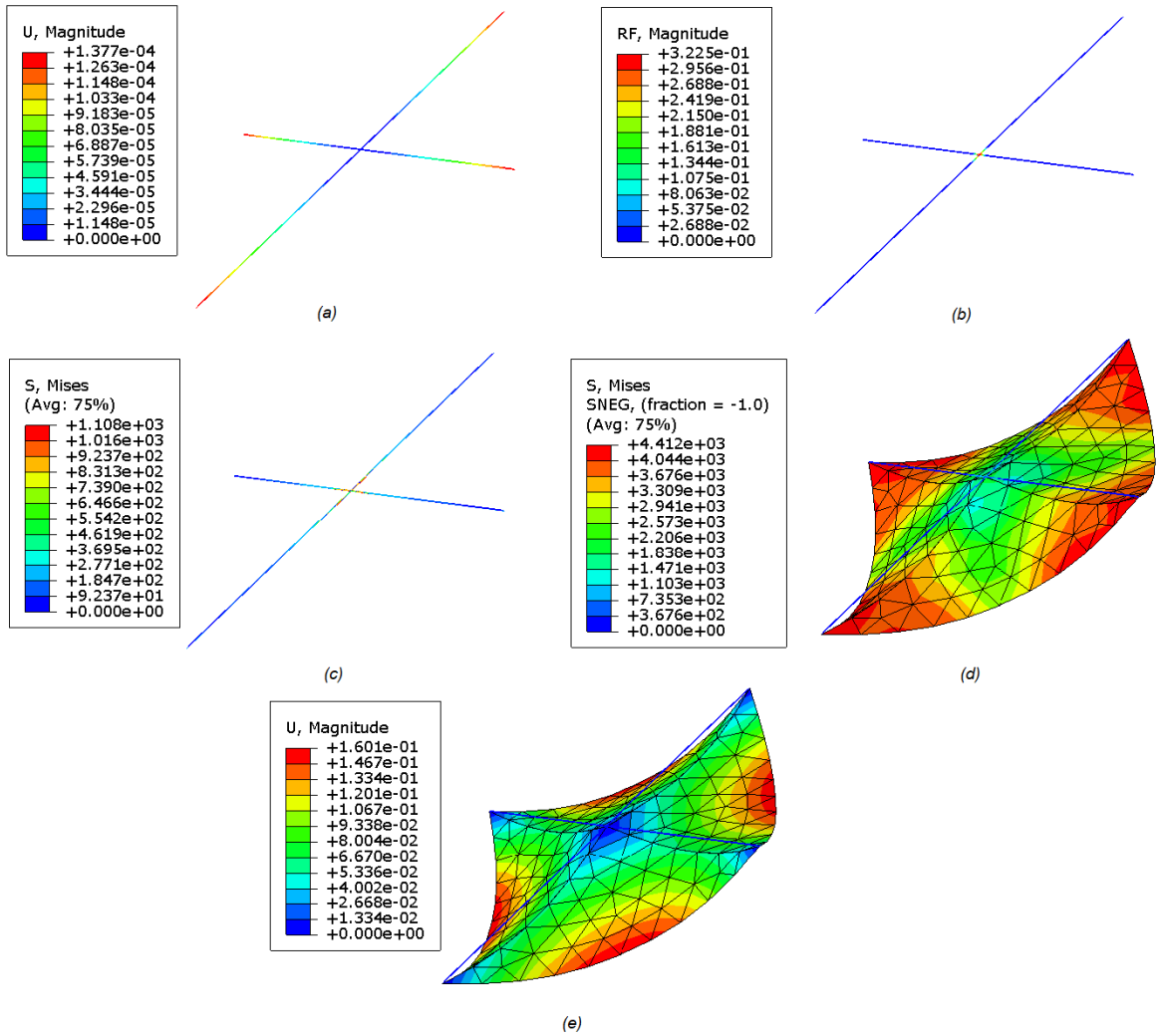

Figure 11. Solar sail analysis near the Venus orbit, where the (a), (b) and (c) illustrations represent the lattice displacement, reaction force and stress respectively; and (d) and (e) the structure stress and displacement.

In this condition, the solar radiation pressure was raised to 17.4 $\mu N/m^2$, leading to a maximum trust force of 7.83 mN, similar magnitude as the one obtained for the IKAROS' solar sail (JAXA's observed a 1.12 millinewtons thrust force on IKAROS' 196 m^2 sail). This new load level resulted in in a maximum displacement magnitude of 137.7 μm at the tip of the lattice structure, almost doubling

the previous displacement condition. Figure 11 shows the reaction force magnitude (RF, Fig.11 (b)), the maximum displacement of the sail and the lattice structure (U, Fig.11 (a) and (e)) and its' stress conditions (S, Fig.11 (c) and (d)). Anew, the instability effects play a major role in the simulation, since the new load magnitude only increase the stress condition noticed near the satellite core.

4.3 Solar Pressure at 0.72AU (Mercury)

The final static simulation consists in a mission near Mercury orbit, 0.34 astronomical units from the sun. This is hypothetical condition considering the extremely harsh environment near the planet orbit, due to its innermost location and temperatures varying between ranging from $-173\,°C$ to $427\,°C$.

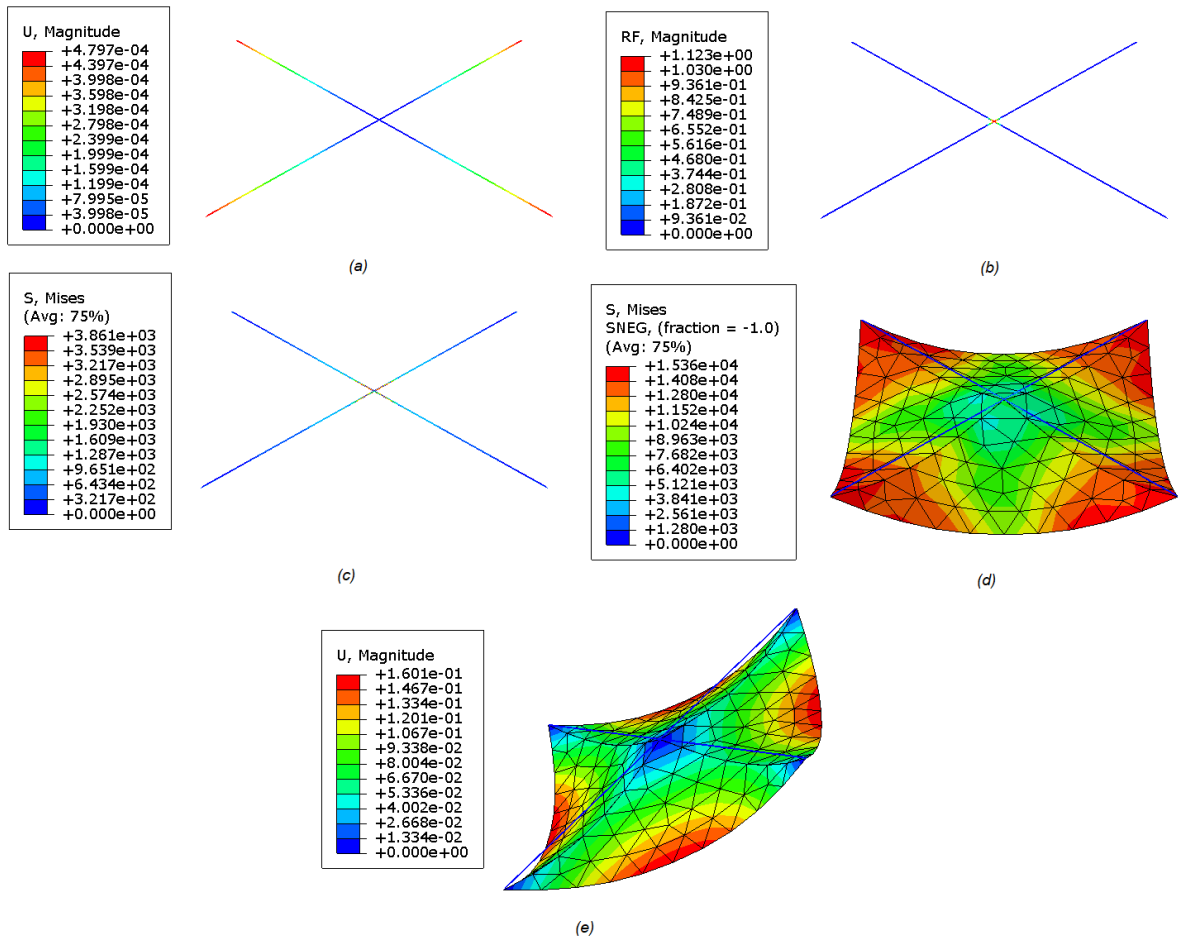

Figure 12. Solar sail analysis near the Mercury orbit, where the (a), (b) and (c) illustrations represent the lattice displacement, reaction force and stress respectively; and (d) and (e) the structure stress and displacement.

Due to its innermost location, Mercury has an average solar radiation pressure value six times higher than the one felt near the Earth's orbit. For a $450\,m^2$ solar sail, this $60.6\,\mu N/m^2$ solar radiation pressure value results in a thrust force of $0.03\,N$, near the thrust range of ion thrusters and some attitude control mechanisms. In this condition, the maximum displacement output is of $0.48\,mm$ at the tip of the lattice structure. Similarly to the previous simulations, Figure 12 shows the reaction force magnitude (RF, Fig.12 (b)), the maximum displacement of the sail and the lattice structure (U, Fig.12 (a) and (e)) and its' stress conditions (S, Fig.12 (c) and (d)).

4.4 Vibration modes

The final simulation performed using the software ABAQUS® consist of a modal analysis of the four-swallow lattice structure. The first eight modes are shown in Figure 13, where we notice that the first four modes correspond to vertical motion, and the four latter to a lateral displacement.

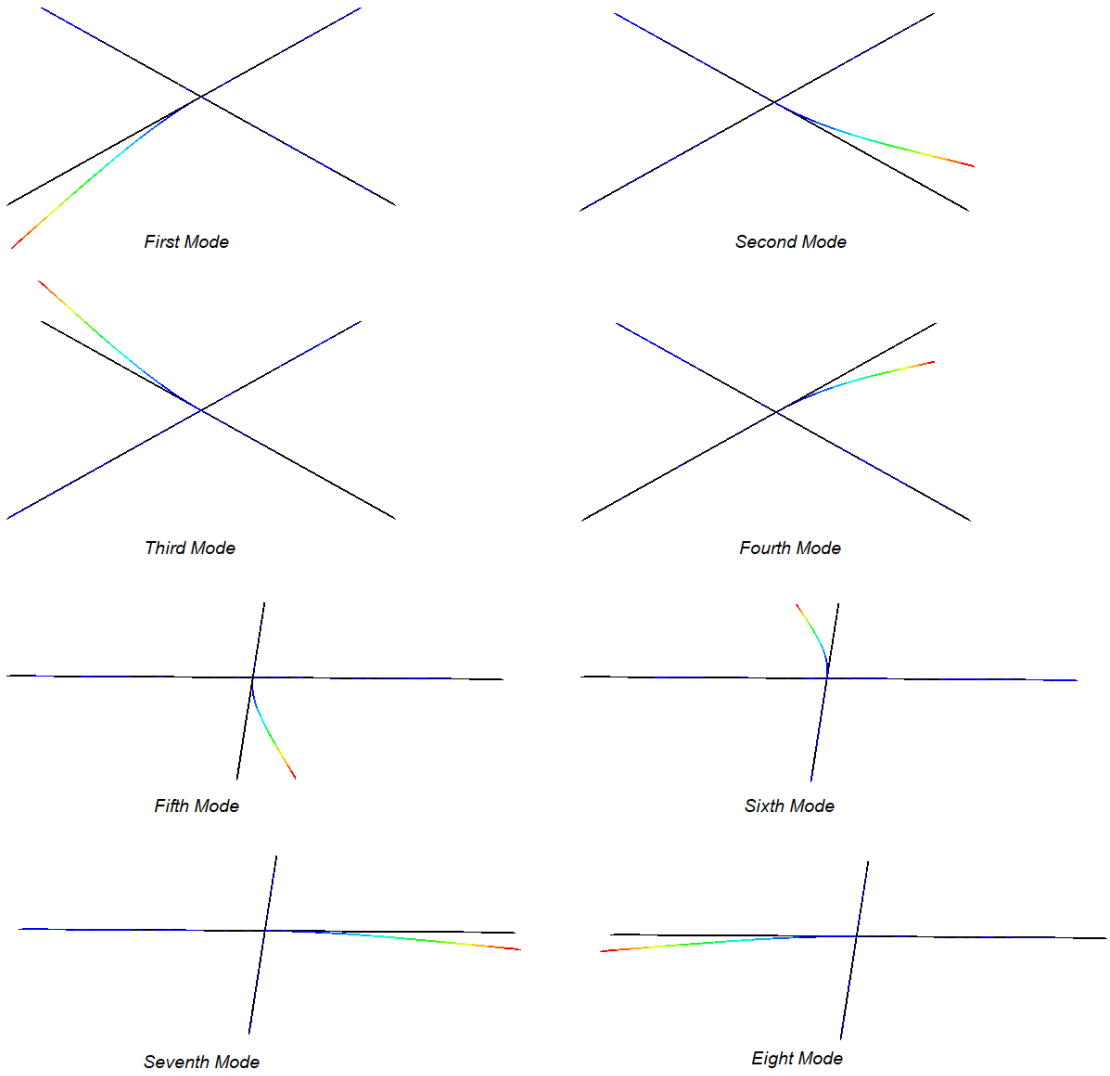

Figure 13. First eight vibration modes of the four-swallow lattice structure.

4.5 Harmonic Vibration

In this section, we present the dynamic simulation of the Lattice structure model, see Fig. 9, undergoing a sine harmonic load. We assume that the base of the lattice structure is fixed in the satellite fuselage, and thus, displacement restricted in the three directions. Furthermore, a harmonic load with magnitude of 1 N is applied at the tip, simulation a hypothetical condition. The MATLAB® version of the implemented model is presented Fig. 14.

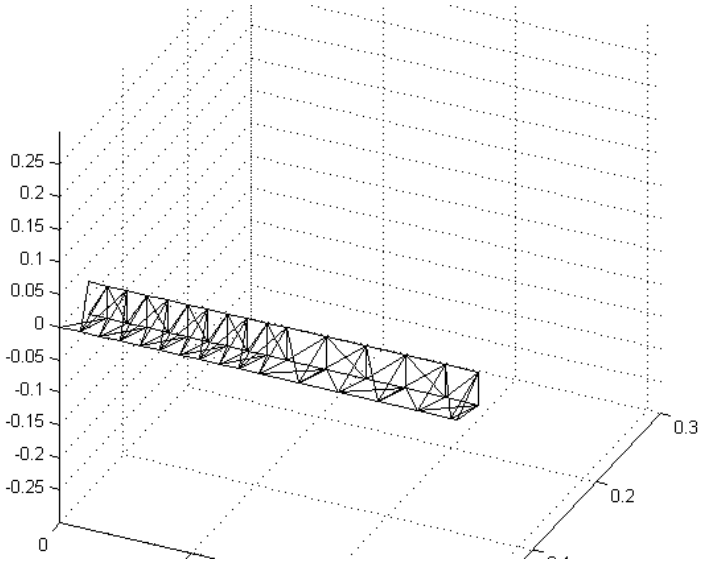

Figure 14. First eight vibration modes of the four-swallow lattice structure.

The applied load is shown in Figure 15, with a maximum amplitude of $1\,N$ and an assumed period of $0.1667\,rad/s$. This harmonic profile was chosen based on a extraordinary load condition (thirty times greater than the solar wind pressure of mercury), to see if any overestimation on the load envelope could lead to structural damage.

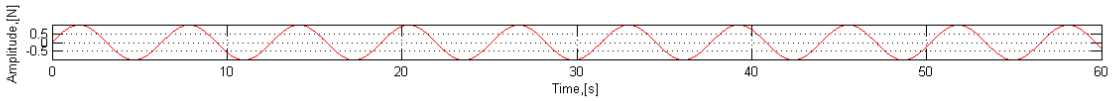

Figure 15. Harmonic load.

For this simulation, we assume an undamped structure, $c = 0$, and build the mass matrix based on mass of each element, computed using the density of Table 1 and the element current length. The displacement at the tip of structure is shown in Figure 16.

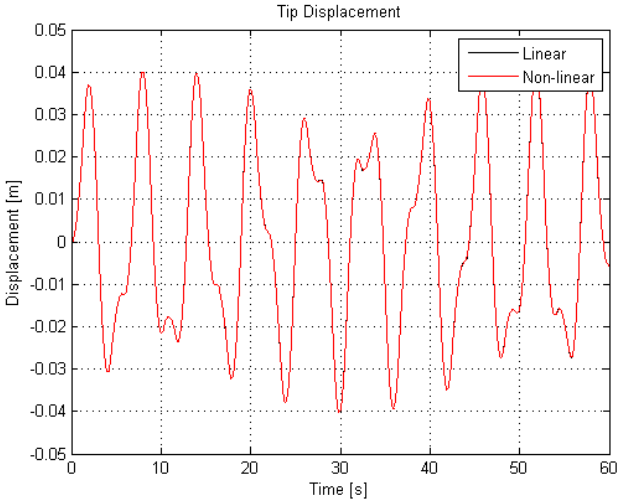

Figure 16. Tip displacement of the lattice structure for the harmonic load.

Complementary, the maximum displacement is like the one obtained from a dynamic simulation using the ABAQUS, as shown in figure 17.

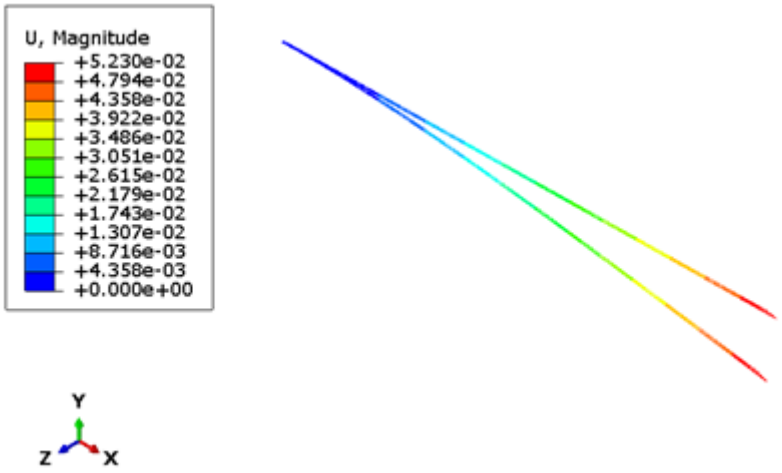

Figure 17. Truss configuration at $t = 2.5s$, ABAQUS simulation.

From these two pictures and the assumption of an extraordinary load condition, became clear that the typical minute load magnitude of the solar wind pressure will not generate enough displacement to clearly affect the linear response.

5 Conclusions

An initial nonlinear dynamic study of a simplified solar sail model was carried out, seeking to understand the main structural limitations of this lightweight appendages as well as to set an adequate procedure to simulate one. Initially, an introduction of some current works in solar sails, as a brief explanation about the used methodology was presented. After that, a static linear/nonlinear analysis was carried out to better understand the load envelope of the lattice structure for three different solar wind pressure configurations, Earth, Venus and Mercury orbits. Finally, we perform a dynamic simulation in order to show that the impact of the nonlinear assumption in the lightweight structure for this load condition is mainly related to the stability of the lattice structure, mainly because of the slenderness ratio of the truss members.

The first part of the results presents the static simulation of the whole structure in three different configurations, an Earth, Venus and Mercury missions. In each one, the displacement and stress are plotted, and used as basis to the stability study of the frame. This was necessary, to prevent buckling of the truss members through the correct positioning of each MgAl rings. After ensuring that the structure configuration could resist the applied load condition, we performed the static and dynamic analysis. Additionally, a modal analysis of the four-swallow lattice structure was carried out and the first eight modes the structures are obtained, noticing that the first four modes correspond are vertical ones, and the four latter lateral.

As shown in the dynamic analysis, the magnitude of the maximum displacement obtained from both simulations, linear and nonlinear one, are nearly identical. A future study will seek implement material nonlinearities and change the load envelope to a combination of attitude correction and solar sailing, seeking to observe if in this configuration the nonlinear assumption leads to noticeable differences. Furthermore, a thermal analysis could also be performed, to observe the thermal effects in the dynamic configuration of the structure.

Acknowledgements

This research was supported by CAPES (Coordenação de Aperfeiçoamento de Pessoal de Nível Superior). The second author also acknowledges support by CNPq.

This study was financed in part by the Coordenação de Aperfeiçoamento de Pessoal de Nível Superior – Brasil (CAPES) – Finance Code 001

References

[1] Tsander, K., From a Scientific Heritage, NASA Technical Translation TTF-541, 1967, a translation of Iz Nauchnogo Naslediya, Nauca Press, Moscow, (1924).

[2] Macdonald, Malcolm & McInnes, Colin. "Solar sail science mission applications and advancement". *Advances in Space Research*. 48. 1702–1716. (2011). 10.1016/j.asr.2011.03.018.

[3] Tsuda, Yuichi & Mori, O & Funase, Ryu & Sawada, H & Yamamoto, T & Saiki, T & Kawaguchi, J. "Flight status of IKAROS deep space solar sail demonstrator". *Acta Astronautica - ACTA ASTRONAUT*. (2011). 69. 833-840. 10.1016/j.actaastro.2011.06.005.

[4] Liu, Jiafu & Cui, Naigang & Shen, Fan & Rong, Siyuan. "Dynamics of highly-flexible solar sail subjected to various forces". *Acta Astronautica*. 103. 55–72. (2014). 10.1016/j.actaastro.2014.06.030.

[5] Boni, L & Mengali, Giovanni & A Quarta, Alessandro. "Solar Sail Structural Analysis via Improved Finite Element Modeling. Proceedings of the Institution of Mechanical Engineers", *Part G Journal of Aerospace Engineering*. (2016). 10.1177/0954410016636164.

[6] Bathe, Klaus-Jürgen & M. Irfan Baig, Mirza. "Conserving energy and momentum in nonlinear dynamics:A simple implicit time integration scheme". *Computers & Structures*, 85, 437-445, 2007.

[7] Crisfield, M. A. *Non-linear Finite Element Analysis of Solids and Structures, Volume 1: Essentials*. John Wiley & Sons, England, (1991).

[8] Crisfield, M. A. *Non-linear Finite Element Analysis of Solids and Structures, Volume 2: Advanced Topics*. John Wiley & Sons, England, (1997).

[9] Carrera, E. "A Study on Arc-length-type Methods and their Operation Failures Illustrated by a Simple Model". *Computers and Structures*, Vol. 50 (2), p. 217-229, (1994).

[10] Souza Lima, V. & Brasil, R. M. L. R. F. "On the Geometrically Nonlinear Analysis of Trusses". In: *Thematic Conference on Computational Methods*, 1998, Barcelona. Proceedings. Barcelona: CIMNE, (1998).

[11] Pimenta, P. M. "Análise Não Linear de Treliças Espaciais", Escola Politécnica da Universidade de São Paulo, Universidade de São Paulo, *Boletim Técnico BT/PEF-8604*, (1983).

[12] Brasil, R.M.L.R.F. *Não-Linearidade Geométrica na Dinâmica de Estruturas Aporticadas Planas: Um Tratamento Pelo Método dos Elementos Finitos*. Thesis (Doutorado em Engenharia Civil) - Universidade de São Paulo (USP), (1990).

[13] Driemeier, L. et.al. "A contribution to the numerical nonlinear analysis of three-dimensional truss systems considering large strains, damage and plasticity". *Communications in Nonlinear Science and Numerical Simulation*, 10, 515:535, (2005).

[14] Krenk, S. *Non-linear Modeling and Analysis of Solids and Structures*. Cambridge: Cambridge University Press, (2009).

[15] Reddy, J. N. *An Introduction to Nonlinear Finite Element Analysis*, Oxford University Press, Oxford, UK, (2004).

[16] Abaqus Unified FEA, Complete solutions for realistic simulation. 3ds Simulia products website: https://www.3ds.com/products-services/simulia/products/abaqus/ Accessed in august 2019.